Journal of Hydrology 558 (2018) 301–313

Contents lists available at ScienceDirect

Journal of Hydrology

journal homepage: www.elsevier.com/locate/jhydrol

Research papers

Quantifying the streamflow response to frozen ground degradation in the source region of the Yellow River within the Budyko framework

Taihua Wang, Hanbo Yang, Dawen Yang *, Yue Qin, Yuhan Wang

State Key Laboratory of Hydroscience and Engineering, Department of Hydraulic Engineering, Tsinghua University, Beijing 100084, China

ARTICLE INFO

Article history:
Received 8 October 2017
Received in revised form 20 December 2017
Accepted 21 January 2018
Available online 3 February 2018
This manuscript was handled by T. McVicar, Editor-in-Chief, with the assistance of Yuting Yang, Associate Editor

Keywords:
Streamflow change
Frozen ground degradation
Budyko framework
Source region of the Yellow River
Tibetan Plateau

ABSTRACT

The source region of the Yellow River (SRYR) is greatly important for water resources throughout the entire Yellow River Basin. Streamflow in the SRYR has experienced great changes over the past few decades, which is closely related to the frozen ground degradation; however, the extent of this influence is still unclear. In this study, the air freezing index (DDF_a) is selected as an indicator for the degree of frozen ground degradation. A water-energy balance equation within the Budyko framework is employed to quantify the streamflow response to the direct impact of climate change, which manifests as changes in the precipitation and potential evapotranspiration, as well as the impact of frozen ground degradation, which can be regarded as part of the indirect impact of climate change. The results show that the direct impact of climate change and the impact of frozen ground degradation can explain 55% and 33%, respectively, of the streamflow decrease for the entire SRYR from Period 1 (1965–1989) to Period 2 (1990–2003). In the permafrost-dominated region upstream of the Jimai hydrological station, the impact of frozen ground degradation can explain 71% of the streamflow decrease. From Period 2 (1990–2003) to Period 3 (2004–2015), the observed streamflow did not increase as much as the precipitation; this could be attributed to the combined effects of increasing potential evapotranspiration and more importantly, frozen ground degradation. Frozen ground degradation could influence streamflow by increasing the groundwater storage when the active layer thickness increases in permafrost-dominated regions. These findings will help develop a better understanding of the impact of frozen ground degradation on water resources in the Tibetan Plateau.

1. Introduction

The Tibetan Plateau (TP), also known as the third pole of the globe, has the largest area of alpine permafrost in the world (Qiu, 2008; Immerzeel et al., 2010; Cuo et al., 2015). Almost all of the TP is underlain by permafrost and seasonally frozen ground because of its high elevation (Guo and Wang, 2013). The TP contains the headwaters of several major Asian rivers, including the Yellow River, Yangtze River, and Brahmaputra River, and these rivers provide water for more than 1.4 billion people (Immerzeel et al., 2010). However, due to limited observations and the complicated interactions between hydrological and cryospheric processes, the responses of streamflow and other eco-hydrological variables to climate change and the consequent cryospheric changes in the TP are not well understood, which has aroused wide concern recently (Cao et al., 2006; Immerzeel et al., 2010; Kang et al., 2010; Yang et al., 2011; Qiu, 2012; Yi et al., 2014; Cuo et al., 2015; Qin et al., 2016; Zhang et al., 2016b; Qin et al., 2017).

The source region of the Yellow River (SRYR) upstream of the Tangnaihai hydrological station is located in the northeastern TP and provides 34.8% of the total water resources of the Yellow River (Hu et al., 2011; Yuan et al., 2015; Qin et al., 2017). Several studies have reported the degradation of frozen ground in the SRYR, including an upward shift in the permafrost lower limit, shifts in the permafrost boundary and a decrease in the maximum frozen depth (Jin et al., 2009; Fang et al., 2011). Frozen ground degradation can influence soil infiltration and drainage, enhance groundwater-surface water interaction and increase the baseflow in many cold regions (Walvoord and Kurylyk, 2016). Bense et al. (2012) suggested a large increase in groundwater discharge to streams in response to permafrost degradation based on numerical simulations for several Arctic rivers. Applying gray relational analysis to the upper Heihe River Basin, northeastern TP, Qin et al. (2016) found that the annual maximum frozen depth was one of the major factors on increases in the baseflow during the cold season. Cuo et al. (2015) discovered that precipitation changes and

* Corresponding author.
E-mail address: yangdw@tsinghua.edu.cn (D. Yang).

https://doi.org/10.1016/j.jhydrol.2018.01.050
0022-1694/

frozen ground degradation enhanced the surface hydrological processes in the northern TP based on Variable Infiltration Capacity (VIC) model simulations. Frozen ground degradation was also found to be associated with a slowdown in winter recession and the flattening of intra-annual streamflow in the SRYR (Niu et al., 2016; Qin et al., 2017; Wang et al., 2017), in northeastern China (Duan et al., 2017a), and in Arctic rivers (Lyon and Destouni, 2010; Walvoord and Kurylyk, 2016).

The influence of frozen ground degradation on annual streamflow, however, is not consistent among different regions. To the best of our knowledge, few quantitative analyses have been employed to investigate the impacts of frozen ground degradation on streamflow in the TP, and the mechanism of the streamflow response to frozen ground degradation is still unclear. Recently, Duan et al. (2017b) quantified the streamflow response to permafrost degradation based on the assumption that an increase in the active layer thickness would increase the annual streamflow in northeastern China. However, many researchers hypothesized that permafrost degradation would decrease the streamflow in the TP by lowering the groundwater table (Cheng and Wu, 2007; Jin et al., 2009; Yang et al., 2010) and enlarging the water storage capacity via an increased thawing depth (Niu et al., 2016). This is different from the hypothesis provided by Duan et al. (2017b) and different from the situation observed for Arctic rivers (Qiu, 2012).

Because of the inconsistency in the streamflow response to frozen ground degradation among different regions, this study does not initially assume whether frozen ground degradation will increase or decrease streamflow. Instead, this study employs the Budyko framework to quantify the streamflow response to frozen ground degradation. The Budyko hypothesis (Budyko, 1974) states that the annual water balance can be expressed as a function of the available water and energy. The Budyko framework has been applied to reflect the impacts of changes in dynamic landscape factors, including vegetation cover (Potter and Zhang, 2009; Donohue et al., 2010; Zhang et al., 2016a), human activities (Xu et al., 2014; Yang et al., 2014; Ning et al., 2017), and snowfall fraction (Berghuijs et al., 2014; Zhang et al., 2015; Barnhart et al., 2016), on annual streamflow. However, the Budyko framework has not yet been extended to quantify the impacts of frozen ground degradation.

A number of previous studies identified a decrease in streamflow in the SRYR during the 1990s (Cao et al., 2006; Zheng et al., 2007). Consequently, numerous attempts have been made to understand the causes of such streamflow variations. Hu et al. (2011) found that the correlation coefficients between the annual precipitation and annual streamflow increase from upstream to downstream and that a decrease in streamflow can be associated with decreasing wet season precipitation and rising temperatures. Utilizing sensitivity-based methods, Zheng et al. (2009) and Zhao et al. (2009) estimated that climate change manifesting as variations in precipitation and potential evapotranspiration contributed to <30% of the streamflow reduction at the Tangnaihai station in the 1990s; they further attributed the other 70% of the streamflow reduction to land use changes and human activities. By employing the VIC model in the SRYR, Cuo et al. (2015) discovered a deviation between observed streamflow and VIC-simulated streamflow values using a static land use map, and they found that the land use-induced deviation expanded during 1960–2000. Streamflow changes that cannot be directly explained by climate factors may also arise from cryospheric changes, such as frozen ground degradation (Cheng and Wu, 2007; Cuo et al., 2015) and variations in the snowfall fraction of the total precipitation (Berghuijs et al., 2014; Zhang et al., 2015), where further investigations are needed.

Recent studies have found that the streamflow trend reversed from decreasing to increasing since the 2000s due to the increasing precipitation. However, the streamflow did not recover as much as precipitation (Meng et al., 2016). Meng et al. (2016) attributed all of the streamflow changes in the 2000s to evapotranspiration changes based on the VIC model. Meanwhile, Xu et al. (2013) highlighted the importance of the increase in the water storage detected by Gravity Recovery and Climate Experiment (GRACE) satellite since 2003. Cuo et al. (2015) claimed that the "Three Rivers Source Region Reserve" project, which was launched in 2003, also played a role in the observed streamflow changes. Such ecological projects have already produced positive effects on grassland restoration on the TP (Xu et al., 2016) and reduced the growing season water yield due to increased evapotranspiration and soil water retention in the source region of the Yangtze River (Li et al., 2017). The impacts of ecological projects on annual streamflow in the SRYR, however, have rarely been analyzed.

In summary, previous studies used sensitivity-based methods or process-based models to analyze the possible reasons for streamflow changes in the SRYR (Zhao et al., 2009; Zheng et al., 2009; Cuo et al., 2015). However, most of these studies included only one change point close to the year 1990, and they did not explain the observed increase in streamflow since the 2000s. While the impacts of frozen ground degradation on streamflow changes were conceptualized in previous investigations, few quantitative analyses have been performed, and thus, the underlying mechanisms are still unclear. Therefore, the objectives of this study are to (1) understand the long-term streamflow changes over the past 50 years in the SRYR, (2) develop a decomposition approach within the Budyko framework to analyze the streamflow response to frozen ground degradation, and (3) use the extended Budyko framework to quantify the direct impact of climate change, manifesting as changes in the precipitation and potential evapotranspiration, as well as the impact of frozen ground degradation on streamflow.

2. Study area and data

2.1. Study area

The SRYR is located in the transitional zone of seasonally frozen ground and permafrost in the northeastern TP (Jin et al., 2009). In this study, the SRYR refers to the upstream catchment above the Tangnaihai hydrological station. The SRYR covers an area of 122,000 km^2 that accounts for 16% of the total area of the Yellow River Basin, and it yields 35% of the total runoff of the Yellow River (Hu et al., 2011). The elevation of the SRYR ranges from 2656 m to 6350 m (Fig. 1) and decreases from the southwest to the northeast. The Zoige wetland, which is located in the southeastern SRYR, is one of the largest alpine wetlands in the TP, and it is dominated by helophyte species (Zhang et al., 2016b).

2.2. Data

Digital elevation data with a resolution of 90 m were obtained from the Shuttle Radar Topography Mission (SRTM) (Jarvis et al., 2008). Daily mean air temperature, wind speed, daily average relative humidity and sunshine hour data from the 22 meteorological stations (Fig. 1) located within and around the SRYR were downloaded from the China Meteorological Administration (CMA) (http://data.cma.cn). An angular distance weighting method with elevation corrections (Yang et al., 2004) was utilized to produce 1-km gridded datasets on a daily basis.

The gridded precipitation data were spatially interpolated from gauge observations using the climatology-based optimal method proposed by Shen and Xiong (2016). The fraction of precipitation falling as snow (f_s) was estimated using a single temperature

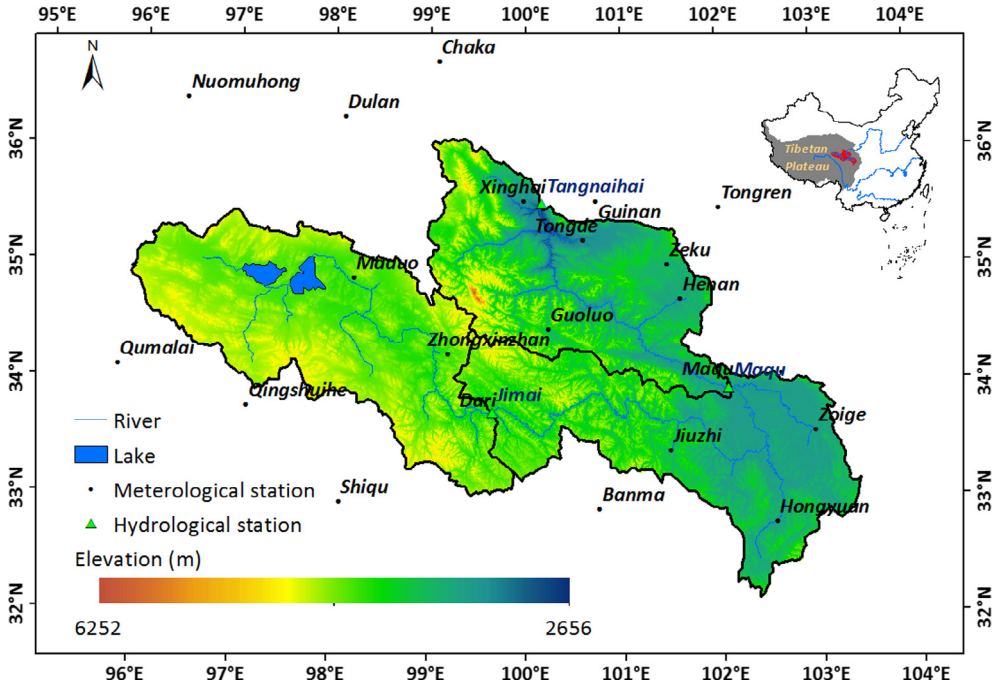

Fig. 1. Study area and locations of the meteorological and hydrological stations.

threshold method. If the daily mean air temperature is lower than 1 °C, then the daily precipitation is considered to be entirely snowfall, and vice versa (Sato et al., 2008; Zhang et al., 2008; Berghuijs et al., 2014). To minimize the effects of carry over storage of snowfall, all of the annual values used in this study are from 1 September to 31 August as a hydrologic year. The multi-year average snowfall fraction (f_s) is 0.19 for the SRYR (Table 1), which is similar to other estimates in this region (Sato et al., 2008; Hu et al., 2011). The daily potential evapotranspiration (E_0) was calculated based on the Penman equation as recommended by Shuttleworth (1993). Details regarding the equations and procedures used to calculate E_0 can be found in Yang et al. (2007) and Zhang et al. (2015).

The leaf area index (LAI3g) dataset and the fraction of photosynthetically active radiation absorbed by vegetation (FPAR3g) dataset, both of which were derived from the 3rd generation of the normalized difference vegetation index (NDVI3g) of the Global Inventory Modeling and Mapping Studies (GIMMS) (Zhu et al., 2013), were adopted in this study. The LAI3g and FPAR3g datasets both have a 15-day temporal resolution and a 1/12° (0.0833°) spatial resolution, and they are available from July 1981 to December 2011.

Monthly streamflow data from the Jimai, Maqu and Tangnaihai hydrological stations are available during 1965–2015. In this study, the SRYR is divided into 3 sub-regions according to the locations of the 3 hydrological stations: (1) the region upstream of Jimai (JM), (2) the region between Jimai and Maqu (JM-MQ), and (3) the region between Maqu and Tangnaihai (MQ-TNH) (see Figs. 1 and 2). To obtain the runoff depths in JM-MQ and MQ-TNH, the runoff volume at the upper stream station was subtracted from the runoff volume at the lower stream station, and the resulting difference was then divided by the area of the sub-region between the two stations.

According to the Map of Permafrost on the Qinghai-Tibetan Plateau (1:3,000,000 scale) complied by the Institute of Geographic Science, Chinese Academy of Sciences (IGS/CAS) (Ran et al., 2012) (Fig. 2), JM has the largest proportion of permafrost (63.0%), while JM-MQ has the smallest proportion of permafrost (8.7%) (Table 1). The multi-year average climatic, hydrologic and vegetation characteristics and the permafrost information for the 3 sub-regions and the entire SRYR are shown in Table 1. JM represents a permafrost-dominated area, while JM-MQ and MQ-TNH represent seasonally frozen ground-dominated areas, of which JM-MQ has a denser vegetation cover.

This study adopts two evapotranspiration (*ET*) products (Fig. 3) to investigate the possible mechanism of the impact of frozen ground degradation on streamflow. The first *ET* product is the

Table 1
The multi-year average climatic, hydrologic, vegetation and permafrost characteristics in SRYR.

	JM	JM-MQ	MQ-TNH	SRYR
Basin area (km^2)	45,300	41,020	37,370	123,690
Annual runoff (mm) (Q)	91.6	249.1	158.2	164.0
Annual precipitation (mm) (P)	451.2	674.1	507.4	542.1
Annual potential evapotranspiration (mm) (E_0)	745.4	734.8	754.7	744.7
Mean annual air temperature (°C) (T_a)	−3.6	−0.6	−1.6	−2.0
Runoff ratio	0.20	0.37	0.31	0.30
Snowfall fraction (f_s)	0.24	0.17	0.17	0.19
Mean annual leaf area index (*LAI*)	0.42	0.94	0.73	0.69
Permafrost area proportion	63.0%	8.7%	26.6%	34.0%

Note: JM = the region in the upstream of Jimai, JM-MQ = Jimai to Maqu, MQ-TNH = Maqu to Tangnaihai, SRYR = the entire source region of Yellow River in the upstream of Tangnaihai.

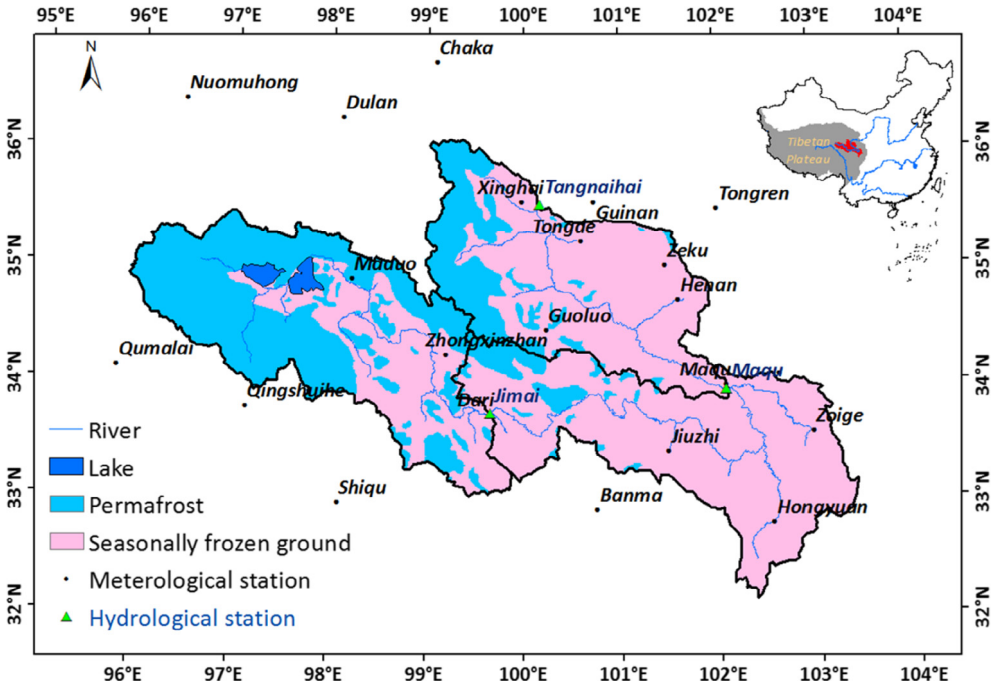

Fig. 2. Permafrost distribution of the source region of Yellow River (SRYR).

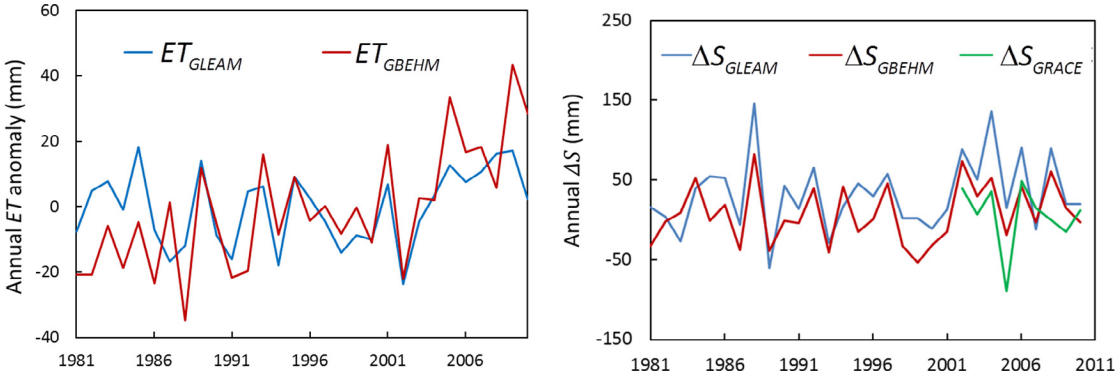

Fig. 3. Comparison of annual *ET* anomaly from GLEAM, GBEHM, and annual water storage change (ΔS) derived from GLEAM, GBEHM and GRACE during 1981–2010 in the entire SRYR.

Global Land Evaporation Amsterdam Model (GLEAM), a global dataset with a 0.25° resolution spanning 1980–2016 that uses a Priestley-Taylor approach to calculate E_0 and integrates point-wise *ET* observations at FLUXNET sites with reanalysis data and satellite-based information (Miralles et al., 2014; Zhang et al., 2016c). The second *ET* product was calculated using a geomorphology-based eco-hydrological model (GBEHM) that was specifically calibrated and calculated for the SRYR with a 3-km resolution during 1981–2011 (Qin et al., 2017). GBEHM is a distributed hydrological model that can be used for the simulation of hydrological processes in cold regions (Gao et al., 2016). The transpiration rate in GBEHM is calculated using the same algorithm as the SiB2 model, and FPAR data are used in the transpiration calculation. More details can be found in Gao et al. (2016) and Qin et al. (2017). The annual *ET* anomaly series derived from GLEAM and GBEHM in the SRYR show similar inter-annual variabilities with a correlation coefficient (r) of 0.61 (Fig. 3).

The annual water storage change (ΔS) derived from these two *ET* products are also compared with the GRACE-derived water storage change (ΔS_{GRACE}). The annual *ET* derived from either GLEAM or GBEHM can then be used to obtain ΔS by utilizing the water balance equation:

$$\Delta S_{GLEAM,i} = P_{GLEAM,i} - Q_i - ET_{GLEAM,i} \quad (1a)$$

$$\Delta S_{GBEHM,i} = P_{GBEHM,i} - Q_i - ET_{GBEHM,i} \quad (1b)$$

where P_i and Q_i represent the annual precipitation and streamflow in the hydrologic year *i*. P_i is different between the two products since GLEAM uses the Multi-Source Weighted-Ensemble Precipitation (MSWEP) dataset for its precipitation forcing (Beck et al., 2017), while GBEHM adopts gridded precipitation data spatially interpolated from gauge observations using the method proposed by Shen and Xiong (2016). Terrestrial water storage anomaly (TWSA) data derived using GRACE satellite data from the Center for Space Research (CSR) for 2002–2015 were downloaded with a resolution of 1° (Landerer and Swenson, 2012) (https://grace.jpl.nasa.gov/data/get-data/monthly-mass-grids-land/). The TWSA time series for the SRYR were derived using an area-weighting method and filtered using a 3-month moving average method (Xu et al.,

2013). The value of ΔS_{GRACE} during the hydrologic year i, which starts in September, can be estimated as follows (Xu et al., 2013):

$$\Delta S_{GRACE,i} = TWSA_{September,i+1} - TWSA_{September,i} \quad (2)$$

Fig. 3 shows that the ΔS time series derived from GLEAM (ΔS_{GLEAM}), GBEHM (ΔS_{GBEHM}) and GRACE (ΔS_{GRACE}) are similar with regard to their amplitudes and annual fluctuations, indicating that these *ET* products are reliable in the SRYR.

3. Methods

3.1. Attribution analysis within the Budyko framework

Water storage changes generally cannot be ignored at the annual scale (i.e., $\Delta S_i \neq 0$), and thus, the water balance equation is expressed as follows:

$$Q = P - ET - \Delta S \quad (3)$$

where Q, P, ET, and ΔS respectively represent the observed annual streamflow, precipitation, actual evapotranspiration and water storage change (unit: mm).

The Budyko hypothesis (Budyko, 1974) states that the annual water balance can be expressed as a function of the available water and energy, and it assumes that the ratio of actual evapotranspiration to precipitation (ET/P) is a function of the aridity index ($\phi = E_0/P$):

$$ET/P = F(\phi) \quad (4)$$

Different forms of $F(\phi)$ have been proposed under the Budyko framework (Schreiber, 1904; Ol'Dekop, 1911; Pike, 1964; Budyko, 1974; Fu, 1981; Zhang et al., 2001; Yang et al., 2008; Zhou et al., 2015b). Based on dimensional analysis and mathematical reasoning, Yang et al. (2008) derived the water-energy balance equation analytically, which is expressed as Eq. (5) and is known as the Choudhury-Yang equation:

$$ET_{Budyko} = PE_0/(P^n + E_0^n)^{1/n} \quad (5a)$$

$$F(\phi) = (\phi^{-n} + 1)^{-1/n} \quad (5b)$$

where the annual precipitation (P) and annual E_0 respectively represent the available water and the available energy, and the parameter n represents the catchment characteristics, which are mainly related to properties of the soil, topography and vegetation (Yang et al., 2007; Zhou et al., 2015a; Zhang et al., 2016a).

If the annual *ET* and *Q* are determined only by climate factors, they should be exactly the same as their corresponding Budyko-estimated values. Ignoring ΔS, the streamflow estimated using the Budyko curve should be as follows:

$$Q_{Budyko} = f(P, E_0, n) = P - ET_{Budyko} = P - PE_0/(P^n + E_0^n)^{1/n} \quad (6)$$

We assume that the long-term average of the observed annual streamflow is equal to the Budyko-based estimated streamflow. Thus, by using long-term averages of the observed annual streamflow, precipitation and E_0, the catchment parameter (n) can be calculated. At the annual scale, however, a deviation exists between the observed annual Q and Q_{Budyko}. Eq. (3) can be rewritten as follows:

$$\begin{aligned} Q &= P - (ET_{Budyko} + ET_{dev}) - \Delta S \\ &= (P - ET_{Budyko}) + (-ET_{dev} - \Delta S) = Q_{Budyko} + Q_{dev} \end{aligned} \quad (7)$$

where Q_{dev} is the deviation of the observed annual Q from Q_{Budyko} ($Q_{dev} = Q - Q_{Budyko}$). Q_{dev} includes two components ($Q_{dev} = -ET_{dev} - \Delta S$): the deviation of *ET* from the Budyko-estimated *ET* ($ET_{dev} = ET - ET_{Budyko}$) and the water storage change (ΔS). It is caused by the landscape factors including frozen ground and vegetation, and can be written as a function of these factors. Frozen ground measurements are rare and are usually restricted to point-scale estimates in frozen ground regions. Therefore, the air freezing index (DDF_a) is selected as the indicator for frozen ground degradation in this study, and it is calculated using the following equation (Frauenfeld et al., 2007):

$$DDF_a = \sum_{j=1}^{N_F} |T_j|, T_j < 0^\circ C \quad (8)$$

where N_F is the number of days with an air temperature below 0 °C in a given hydrologic year, j = 1, 2,. . ., N_F, and T_j is the daily mean air temperature (°C) on a specific day j. More details about the selection of DDF_a as an indicator for the degree of frozen ground degradation will be discussed in Section 5.1.

If we assume that DDF_a is independent of other landscape factors, we have the following equation:

$$Q_{dev} = g(DDF_a) + h(other\ landscape\ factors) \quad (9)$$

The shape of $g(DDF_a)$ reflects the relationship between frozen ground and streamflow, and it is fitted using 5-year sequential averages of Q_{dev} and DDF_a in this study (Yang et al., 2016). For each variable, ten samples of the 5-year means are yielded during 1965–2014 (i.e., 1965–1969, 1970–1974,. . ., 2010–2014). From Eq. (7), the long-term streamflow change between two periods (ΔQ) can be attributed to the direct impact of climate change (ΔQ_c) and the impact of landscape change (ΔQ_l):

$$\Delta Q = \Delta Q_{Budyko} + \Delta Q_{dev} = \Delta Q_c + \Delta Q_l \quad (10)$$

If we set the parameter n in Eq. (5) time-invariant in a certain region, then $\Delta Q_{Budyko} = \Delta Q_c$, and all the landscape-induced streamflow change are remained in ΔQ_{dev} thus $\Delta Q_{dev} = \Delta Q_l$. The climate contribution to streamflow changes can be estimated via the climate elasticity method (Zheng et al., 2009; Wang and Hejazi, 2011; Yang and Yang, 2011; Xu et al., 2014; Yang et al., 2014). The precipitation elasticity of streamflow (ε_P) is defined as $\varepsilon_P = \frac{dQ/Q}{dP/P}$, and the potential evapotranspiration elasticity of streamflow (ε_{E_0}) is defined as $\varepsilon_{E_0} = \frac{dQ/Q}{dE_0/E_0}$. Thus, the climate-induced streamflow change (ΔQ_c) can be estimated by:

$$\Delta Q_c = \Delta Q_P + \Delta Q_{E_0} = \varepsilon_P \frac{\Delta P}{P} Q + \varepsilon_{E_0} \frac{\Delta E_0}{E_0} Q \quad (11)$$

Following the derivation process described by Arora (2002), the climate elasticity of streamflow (i.e., ε_P and ε_{E_0}) can be expressed as follows:

$$\varepsilon_{E_0} = -\phi F'(\phi)/[1 - F(\phi)] \quad (12a)$$

$$\varepsilon_P = 1 + \phi F'(\phi)/[1 - F(\phi)] \quad (12b)$$

Combining Eq. (12) with the Choudhury-Yang equation shown in Eq. (5b), the climate elasticity of streamflow can be calculated by the long-term aridity index (ϕ). Climate-induced streamflow change (ΔQ_c) can be obtained using Eq. (12) and the remaining term is attributed to landscape change (ΔQ_1).

The landscape-induced streamflow change (ΔQ_l) can be further attributed to frozen ground degradation (ΔQ_f) and land use changes (ΔQ_{lu}):

$$\Delta Q_l = \Delta Q_f + \Delta Q_{lu} \quad (13)$$

The streamflow change caused by frozen ground degradation (ΔQ_f) can be calculated by Eq. (14) and the remaining term is attributed to land use changes (ΔQ_{lu})

$$\Delta Q_f = \Delta g(DDF_a) = g(DDF_{a,2}) - g(DDF_{a,1}) \quad (14)$$

where $DDF_{a,1}$ and $DDF_{a,2}$ are the mean air freezing indices during two different periods. In this study, climate-induced streamflow change (ΔQ_c) represents the direct impact of climate change manifesting as changes in both precipitation and E_0, while the impact of frozen ground degradation on streamflow (ΔQ_f) can be regarded as part of the indirect impact of climate change.

3.2. Change point and trend detection

In this study, the moving *t*-test was adopted to detect change points within the streamflow time series. The *t*-test assesses whether the means of two subsamples are significantly different from one another. The formula for the *t*-test is as follows (Zheng et al., 2007; Yin et al., 2015):

$$t = \frac{\overline{x_1} - \overline{x_2}}{s\sqrt{\frac{1}{n_1} + \frac{1}{n_2}}} \tag{15}$$

$$s = \sqrt{\frac{n_1 s_1^2 + n_2 s_2^2}{n_1 + n_2 - 2}} \tag{16}$$

where $\overline{x_i}$, s, and n_i are the mean, standard deviation and size of the two independent samples ($i = 1, 2$). The *t*-test has $n_1 + n_2 - 2$ degrees of freedom. The moving *t*-test applies the *t*-test to a subseries with a fixed length n before and after the potential change points ($n = n_1 = n_2$). If the calculated *t*-value is larger than the critical value t_α, then the point is accepted as a change point at the significance level α. In this study, $n = 10$ and $\alpha = 0.05$, and thus, the critical value is $t_\alpha = 2.1$.

The Mann-Kendall nonparametric test is applied in this study to detect the significance of a trend in the long-term time series (Yang et al., 2004), and a significance level of 0.05 is chosen for all trend analyses in this study.

4. Results

4.1. Long-term streamflow variations

The long-term inter-annual streamflow and precipitation variabilities are shown in Fig. 4. The annual streamflow in all subregions of the SRYR showed decreasing trends during 1965–2015, and the decreasing trend in JM-MQ was significant at the 0.05 significance level (−12.26 mm/10a) (Table 2). In contrast, the annual precipitation among all of the sub-regions of the SRYR showed increasing trends during 1965–2015, except for JM-MQ where the annual precipitation decreased slightly (-1.04 mm/10a). For the entire SRYR, the annual streamflow showed an insignificant decreasing trend (-6.51 mm/10a) during 1965–2015 in contrast to an insignificant annual precipitation increasing trend (+6.48 mm/10a), resulting in a significant decrease in the runoff ratio (-0.01/10a) over the past 50 years at the 0.05 significance level (Table 2).

Two abrupt change points in the annual streamflow in the SRYR were detected using the moving *t*-test, which were respectively 1989 and 2003 (Fig. 5). Thus the past 50 years can be divided into 3 periods: Period 1 (P1, 1965–1989), Period 2 (P2, 1990–2003) and Period 3 (P3, 2004–2015). The abrupt change points of the annual streamflow are similar to the change points of the annual precipitation (Fig. 5).

During P1, the streamflow and precipitation among all of the sub-regions fluctuated around the multi-year average and increased insignificantly at the 0.05 significance level (Fig. 4). While during P2, nearly all of the sub-regions experienced a decrease in both streamflow and precipitation, and the streamflow decreasing rate (−22.47 mm/10a) was larger than precipitation decreasing rate (−9.68 mm/10a). The mean annual streamflow and precipitation values during the three periods are also indicated in Fig. 4. The decrease in the annual streamflow value between P1 and P2 was larger than the decrease in the annual precipitation except within MQ-TNH.

During P3, the annual precipitation trends in all of the subregions except MQ-TNH reversed and started to increase, and the annual streamflow throughout the entire SRYR also increased slightly (+2.67 mm/10a) (Table 2). The precipitation in all of the SRYR sub-regions during P3 exceeded their multi-year averages. However, the streamflow in all of these sub-regions during P3 did not recover as much as the precipitation; instead, the streamflow returned only approximately to the multi-year average value in P3 and was even lower than the average value in P1 (Fig. 4). The runoff ratio exhibited the most rapid decrease during P2 (−0.04/10a), during which time the mean annual air temperature increased by 0.98 °C/10a throughout the entire SRYR (Table 2).

4.2. Decomposition into climate- and landscape-induced streamflow changes

The values of the catchment parameter (n), precipitation elasticity of streamflow (ε_P) and potential evapotranspiration elasticity of streamflow (ε_{E_0}) are shown in Table 3. The results show that the streamflow in permafrost dominated JM is more sensitive to climate factors compared with the other two sub-regions; the values of the climate elasticity of streamflow were $\varepsilon_P = 2.20$ and $\varepsilon_{E_0} = -1.20$, which means that a 10% increase in either the precipitation or E_0 will result in a 22% increase or a 12% decrease in streamflow at JM, respectively.

Attribution analysis of the streamflow changes between different periods was conducted based on the climate elasticity (Table 4). From P1 to P2, the direct impact of climate change can explain only 55.0% of the streamflow decrease, while landscape changes can explain another 45.0% of the streamflow decrease for the entire SRYR. The direct impact of climate change can explain only 21.3% of the streamflow decrease in the permafrost-dominated JM and 69.5% of the streamflow decrease in the seasonally frozen ground-dominated MQ-TNH; meanwhile, 78.7% and 30.5% of the streamflow decreases in JM and MQ-TNH were caused by landscape changes, which is similar to the results of previous studies (Zhao et al., 2009; Zheng et al., 2009).

From P2 to P3, the 83.7 mm increase in precipitation for the entire SRYR caused a 48.1 mm increase in streamflow, while the increase in E_0 led to a 5.1 mm decrease in streamflow. Therefore, the climate-induced increase in streamflow (ΔQ_c) was 43.0 mm, but the observed streamflow only increased by 34.1 mm (Table 4). This indicates that landscape changes had a negative effect on streamflow ($\Delta Q_l < 0$), which was true for all of the sub-regions of the SRYR and for both P1-P2 and P2-P3. The streamflow decrease caused by landscape factors was 21.1 mm from P1 to P2 and 8.9 mm from P2 to P3 for the entire SRYR.

4.3. Streamflow response to frozen ground degradation

The shape of $g(DDF_a)$ in Eq. (9) reflects the relationship between frozen ground and streamflow. From the scatter plots of the 5-year sequential average of Q_{dev} vs that of DDF_a shown in Fig. 6, the relationship between Q_{dev} and DDF_a can be described using a power function:

$$g(DDF_a) = a[(DDF_a - b)/c]^d + e \tag{17}$$

The values of the parameters a, b, c, d, and e were determined via a least squares method, and the fitted equations are labeled in Fig. 6. The values of the coefficients of determination (R^2) were

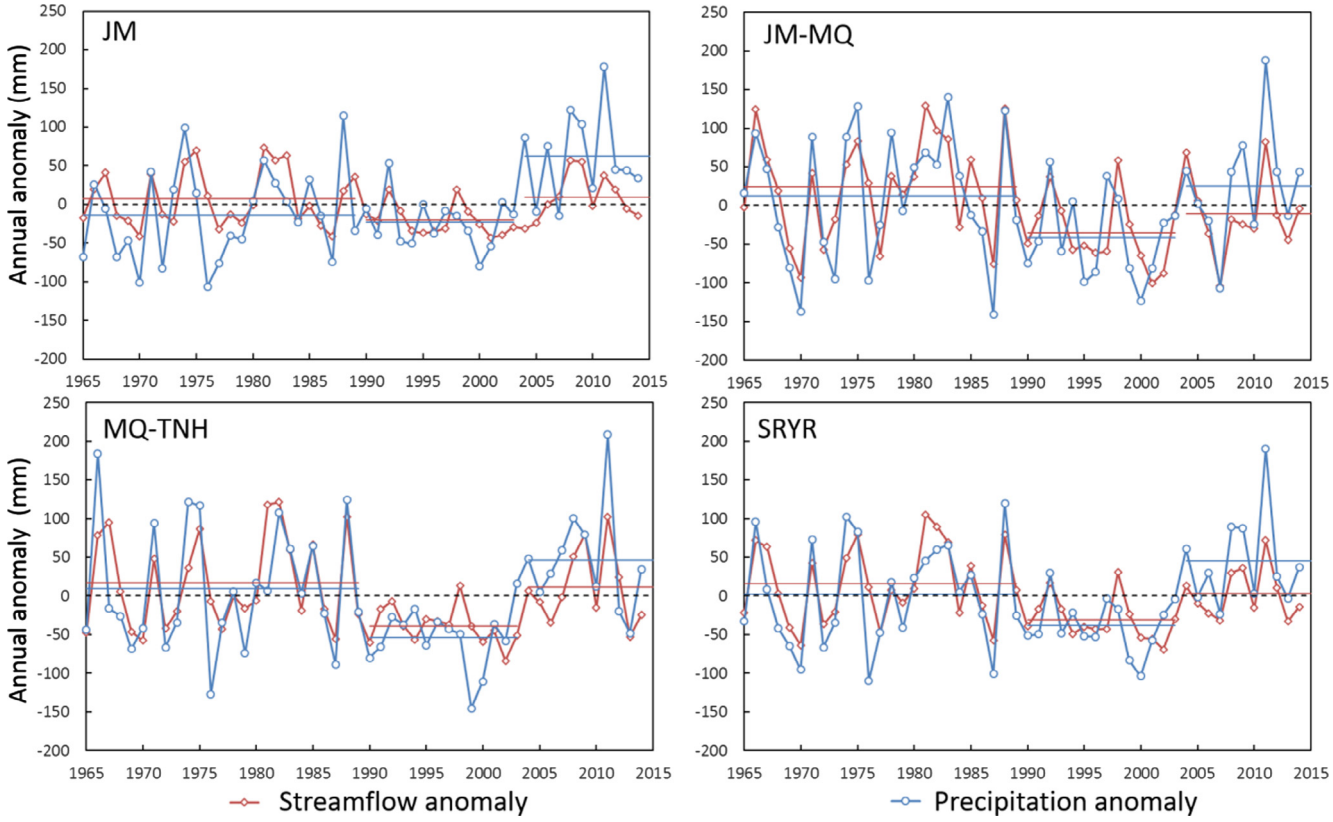

Fig. 4. Annual streamflow and precipitation anomaly in SRYR.

Table 2
Trends of annual streamflow, precipitation and runoff ratio in different periods in SRYR.

		Annual streamflow (mm)				Annual precipitation (mm)				Runoff ratio			
		JM	JM-MQ	MQ-TNH	SRYR	JM	JM-MQ	MQ-TNH	SRYR	JM	JM-MQ	MQ-TNH	SRYR
Trend (mm/10a or /10a)	1965–2015	−2.10	−12.26*	−5.64	−6.51	17.00*	−1.04	1.97	6.48	−0.01	−0.02*	−0.01	−0.01*
	Period 1	3.66	11.52	8.64	7.77	19.18	7.67	4.58	10.95	0.00	0.01	0.01	0.01
	Period 2	−17.83	−32.25	−19.52	−22.47*	−16.67	−13.52	3.01	−9.68	−0.03	−0.04	−0.04	−0.04
	Period 3	19.42	−12.27	−1.22	2.67	13.50	58.44	−19.92	18.31	0.03	−0.04	0.00	−0.01

Note: Trends with an asterisk (*) are significant at a level of 0.05. Annual streamflow is expressed by runoff depth (unit: mm), which is the ratio of runoff volume (unit: m^3) to catchment area (unit: km^2). In JM-MQ and MQ-TNH, the runoff volume of the upper stream station was subtracted from the runoff volume of the lower stream station and then divided by the area of the sub-region between the two stations.

0.38 to 0.63 for the three sub-regions and 0.72 for the entire SRYR, indicating that the fitted power function curves are effective for reflecting the relationship between streamflow and frozen ground in the SRYR.

Combining the equations of $g(DDF_a)$ and Eq. (14), Table 4 can be extended into Table 5, which further decomposes landscape-induced streamflow changes (ΔQ_l) into the parts attributed to frozen ground degradation (ΔQ_f) and land use change (ΔQ_{lu}). The impacts of climate change and frozen ground degradation can explain almost all of the streamflow changes in the SRYR since the values of $(\Delta Q_c + \Delta Q_f)/\Delta Q$ are close to 100% (Table 5).

The results show that from P1 to P2, frozen ground degradation manifesting as a decrease in DDF_a can explain 70.7% of the streamflow decrease in the permafrost-dominated JM and more than 20% of the streamflow decrease in the seasonally frozen ground-dominated JM-MQ and MQ-TNH. For the entire SRYR, frozen ground degradation caused a 15.3 mm decrease in the annual streamflow, accounting for 32.6% of the total streamflow decrease. The direct impact of climate change and the impact of frozen ground degradation can collectively explain 87.6% of the streamflow change from P1 to P2. Land use changes resulted in a 12.4% decrease in streamflow for the entire SRYR from P1 to P2 that can be attributed to the combined effects of a decrease in grasslands and increases in cultivated land, forest and water bodies (Table 6).

While from P2 to P3, the streamflow is projected to increase by 48.1 mm only considering the effects of precipitation (ΔQ_P = 48.1 mm) for the entire SRYR, while the observed annual streamflow only increased by 34.1 mm (ΔQ = 34.1 mm). The difference can be attributed to the effects of increasing E_0 (ΔQ_{E_0} = −5.1 mm) and more importantly, the frozen ground degradation (ΔQ_f = −13.1 mm) (Tables 4 and 5). The direct impact of climate change and the impact of frozen ground degradation can collectively explain 87.5% of the streamflow change from P2 to P3. The values of ΔQ_{lu} from P2 to P3 were positive and close to zero, which might be related to a decrease in cultivated land area as well as to the establishment of the "Three Rivers Source Region Reserve" in 2003 (Cuo et al., 2015) (Table 6).

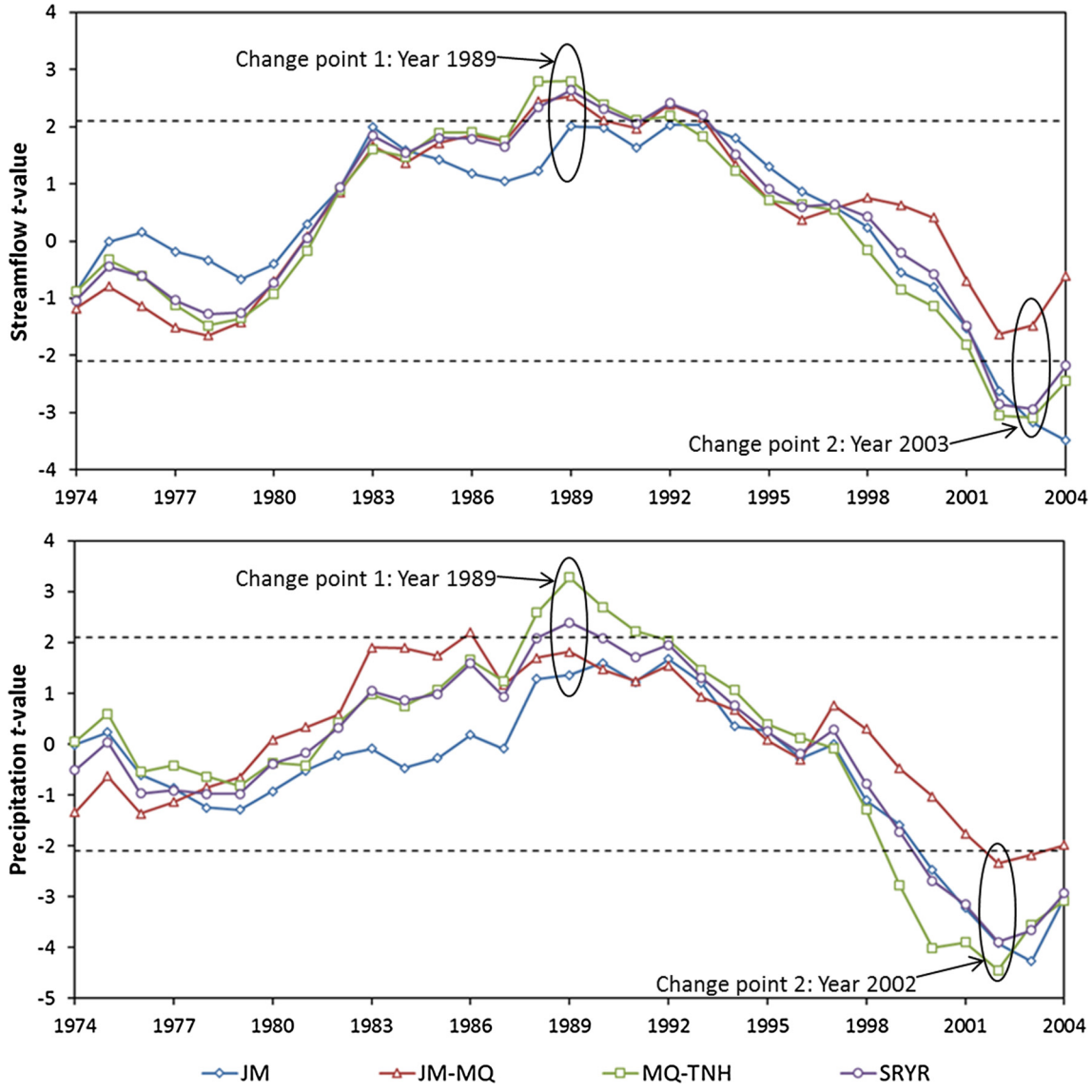

Fig. 5. Change point detection with moving *t*-test for annual streamflow and precipitation.

Table 3
Catchment parameter and climate elasticity of streamflow in SRYR.

	ϕ	n	ε_P	ε_{E_0}
JM	1.65	1.61	2.20	−1.20
JM-MQ	1.09	1.38	1.80	−0.80
MQ-TNH	1.49	1.26	1.83	−0.83
SRYR	1.37	1.38	1.90	−0.90

5. Discussion

5.1. Selection of air freezing index as the indicator of frozen ground degradation

Frozen ground observation is much more difficult than the meteorological observation; hence the frozen ground observations are very rare. Therefore, the air freezing index (DDF_a) and thawing index (DDT_a) are often used to map the permafrost distribution and

Table 4
Attribution analysis of streamflow respectively from Period 1 to Period 2 (P1-P2) and from Period 2 to Period 3 (P2-P3).

		ΔP (mm)	ΔE_0 (mm)	ΔQ (mm)	ΔQ_P (mm)	ΔQ_{E_0} (mm)	ΔQ_c (mm)	ΔQ_I (mm)	$\Delta Q_c/\Delta Q$	$\Delta Q_I/\Delta Q$
P1-P2	JM	−9.4	12.3	−28.3	−4.2	−1.8	−6.0	−22.2	21.3%	78.7%
	JM-MQ	−53.6	11.5	−59.7	−35.7	−3.1	−38.8	−20.9	65.0%	35.0%
	MQ-TNH	−63.3	14.8	−55.6	−36.1	−2.6	−38.6	−17.0	69.5%	30.5%
	SRYR	−40.3	12.8	−46.8	−23.2	−2.5	−25.7	−21.1	55.0%	45.0%
P2-P3	JM	85.7	27.8	29.6	38.3	−4.1	34.2	−4.5	115.3%	−15.3%
	JM-MQ	66.8	29.0	24.5	44.4	−7.9	36.6	−12.1	149.3%	−49.3%
	MQ-TNH	99.7	20.0	50.5	56.8	−3.5	53.3	−2.9	105.6%	−5.6%
	SRYR	83.7	25.8	34.1	48.1	−5.1	43.0	−8.9	126.0%	−26.0%

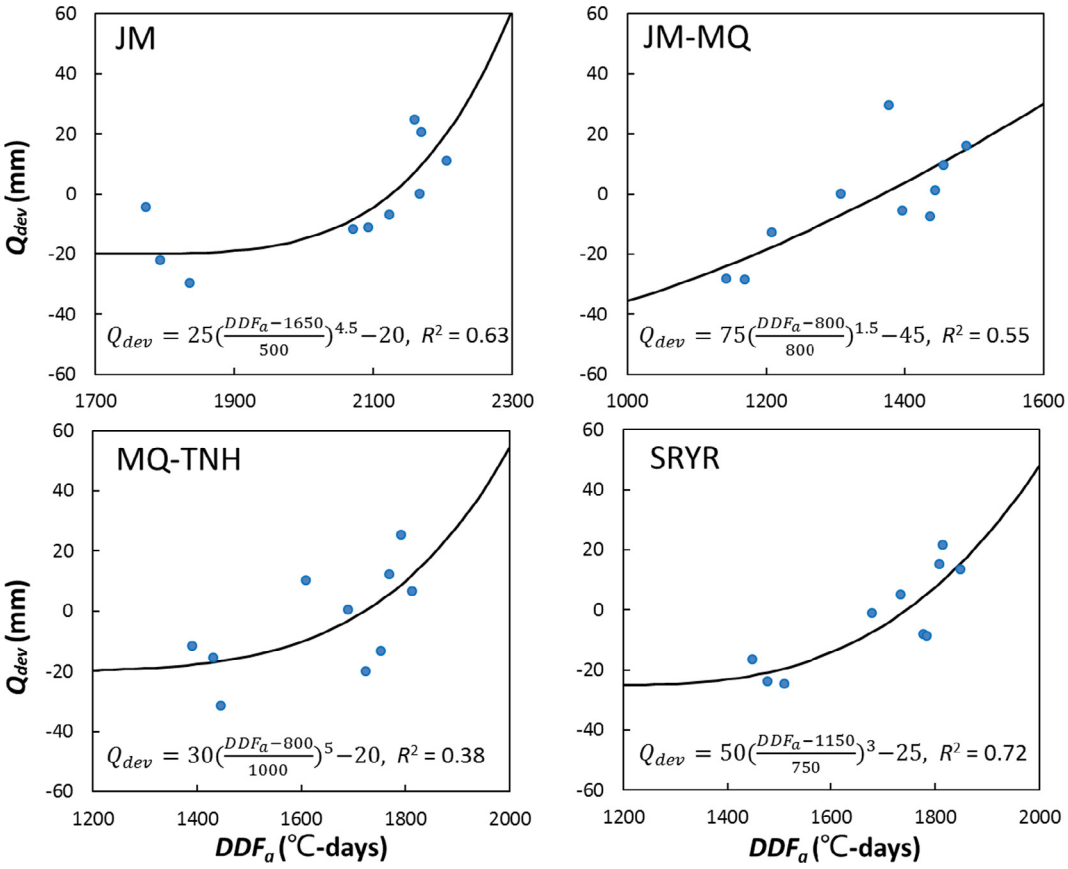

Fig. 6. Scatter plots of annual streamflow deviation (Q_{dev}) vs. air freezing index (DDF_a) in SRYR.

Table 5
Attribution analysis of streamflow considering the contribution of frozen ground and land use changes.

		ΔQ (mm)	$\Delta Q_c/\Delta Q$	ΔDDF_a (°C-days)	ΔQ_f (mm)	$\Delta Q_f/\Delta Q$	$(\Delta Q_c+\Delta Q_f)/\Delta Q$	ΔQ_{lu} (mm)	$\Delta Q_{lu}/\Delta Q$
P1-P2	JM	−28.3	21.3%	−132.3	−20.0	70.7%	92.0%	−2.2	8.0%
	JM-MQ	−59.7	65.0%	−103.5	−12.4	20.8%	85.8%	−8.5	14.2%
	MQ-TNH	−55.6	69.5%	−141.8	−13.3	23.9%	93.4%	−3.7	6.6%
	SRYR	−46.8	55.0%	−125.6	−15.3	32.6%	87.6%	−5.8	12.4%
P2-P3	JM	29.6	115.3%	−243.6	−6.9	−23.2%	92.1%	2.3	7.9%
	JM-MQ	24.5	149.3%	−173.4	−18.1	−73.9%	75.4%	6.0	24.6%
	MQ-TNH	50.5	105.6%	−204.4	−8.3	−16.4%	89.3%	5.4	10.7%
	SRYR	34.1	126.0%	−208.5	−13.1	−38.5%	87.5%	4.3	12.5%

Table 6
Land use change in SRYR expressed by the area proportion of each land use type to the total area.

	P1	P2	P3
Cultivated	0.4%	0.9%	0.4%
Forest	2.6%	6.6%	7.5%
Grassland	89.4%	76.0%	78.2%
Water bodies	1.5%	2.1%	2.2%
Residential	0.0%	0.0%	0.1%
Sandy land or bare land	6.1%	14.3%	11.6%

Note: Data during P1 and P2 were adapted from Zheng et al. (2009), which came from two land use maps of 1986 and 1995 compiled by the Institute of Geographic Sciences and Natural Resources Research (IGSNRR). Data in P3 were derived from the mean values of three land use maps in 2005, 2010 and 2015 downloaded from the Environmental & Ecological Science Data Center for West China (http://westdc.westgis.ac.cn).

predict the ground freeze-thaw state at large scale (Frauenfeld et al., 2007). In this study, we choose the air freezing index (DDF_a) to represent the degree of frozen ground degradation.

The degree of frozen ground degradation is co-determined by multiple variables, including air temperature and other factors, as demonstrated by the Stefan equation (Peng et al., 2017):

$$MTSFG = \sqrt{2\lambda_f n_f / L\rho_l \theta_f}\sqrt{DDF_a} \quad (18)$$

where $MTSFG$ is the maximum thickness of seasonally frozen ground, representing the maximum depth from the ground surface to the freezing front in a freezing season; DDF_a is the air freezing index over a hydrologic year (°C-day); λ_f is the thermal conductivity of frozen soil; n_f is the freezing n-factor which corresponds to the ratio between ground surface and air freezing index and relates to land surface conditions (Klene et al., 2001); L is the latent heat of fusion (3.34×10^5 J kg^{-1}); ρ_l is the density of liquid water (1.00×10^3 kg m^{-3}); θ_f is the volumetric liquid water content before soil freezing. By analyzing freezing depth data across China, Peng et al. (2017) found that DDF_a could account for more than 90% of the variability in $MTSFG$, while no correlation was found between $MTSFG$ and the snow depth.

Due to limited data and relatively stable soil and land surface properties relative to climate forcing, a simplified Stefan equation has been adopted by many studies (Wang et al., 2015; Wu et al., 2015; Peng et al., 2017):

$$MTSFG = E\sqrt{DDF_a} \tag{19}$$

where E is an edaphic parameter representing all of the factors other than DDF_a that influence the freezing depth. The value of E is relatively steady at a certain location, and variations in DDF_a can represent the inter-annual variability in frozen ground degradation.

To illustrate the validity of utilizing DDF_a to represent the degree of frozen ground degradation in the study area, long-term observations of the soil freezing depth at 10 stations in the SRYR during 1967–2015 were obtained from the CMA. A strong correlation between $MTSFG$ and $\sqrt{DDF_a}$ with a mean correlation coefficient (r) value of 0.64 was observed among the 10 stations in the SRYR (Fig. S1).

The degree of frozen ground degradation is directly determined by the soil temperature. Therefore, we calculate the ground freezing index (DDF_g) using observations of the ground surface (0 cm) temperature and the soil temperature at depths of 10 cm, 20 cm and 80 cm at the 10 stations by summing up all of the daily temperatures lower than 0 °C in a given hydrologic year. DDF_a and DDF_g decreased significantly over the past few decades, and the inter-annual variabilities in DDF_a and DDF_g showed a similar pattern (Fig. S2). The value of r between DDF_g at different depths and DDF_a generally decreased with an increase in the soil depth, and most of the corresponding r values are larger than 0.6 (Fig. S3) except at the Maqu, Zoige and Hongyuan stations, where the $MTSFG$ values are relatively small (<100 cm). These results show that DDF_a perform effectively as an indicator for the degree of frozen ground degradation in the SRYR.

In addition to DDF_a, DDT_a is also commonly used as an indicator for estimating the degree of frozen ground degradation (Frauenfeld et al., 2007; Duan et al., 2017a). We also calculate DDT_a by summing up all of the daily temperatures higher than 0 °C in a given hydrologic year. Then, Eq. (9) can be rewritten as follows:

$$Q_{dev} = l(DDT_a) + h(other\ landscape\ factors) \tag{20}$$

The shape of $l(DDT_a)$, which also reflects the relationship between frozen ground degradation and streamflow, was fitted using a 5-year sequential average and DDF_a. From the scatter plots of the 5-year sequential average of Q_{dev} vs that of DDT_a (Fig. S4), the relationship between Q_{dev} and DDT_a can also be described with a similar power function:

$$l(DDT_a) = a[(b - DDT_a)/c]^d + e \tag{21}$$

The values of the parameters a, b, c, d, and e were determined via a least squares method, and the fitted equations are labeled in Fig. S4. From the newly derived function $l(DDT_a)$, we can calculate the streamflow change caused by the frozen ground degradation (ΔQ_f) using the following equation:

$$\Delta Q_f = \Delta l(DDT_a) = l(DDT_{a,2}) - l(DDT_{a,1}). \tag{22}$$

Using DDT_a for different periods (i.e., $DDT_{a,1}$ and $DDT_{a,2}$), we can obtain the streamflow change caused by the frozen ground degradation (ΔQ_f) and the corresponding results (Table S1). The values of ΔQ_f changed only slightly compared with the previous results acquired by selecting DDF_a as the indicator, as is shown in Table 5. Therefore, the relationship between frozen ground degradation and streamflow does not rely much on the choice of the frozen ground index. Hence, the results derived from the proposed method within the Budyko framework are reasonable, and the method is robust.

5.2. Impact of frozen ground degradation on streamflow

The Budyko framework adopted in this study is used for quantifying the direct impact of climate change, manifesting as changes in precipitation and potential evapotranspiration, as well as the impact of frozen ground degradation which, strictly speaking, could be regarded as an indirect impact of climate change. We assume that DDF_a is independent of other landscape factors, and we consequently obtain Eq. (9) to distinguish the impact of frozen ground degradation on the annual streamflow. There are many landscape factors that could cause the deviations between the observed and Budyko-estimated streamflow values (Zhang et al., 2016a). Frozen ground and vegetation in the SRYR have experienced great changes over the past few decades, and they might represent the most prominent landscape factors influencing streamflow. Therefore, we tested the relationship between DDF_a and the LAI, and we did not find a significant correlation.

Based on the results obtained in this study, the direct impact of climate change can explain only 21.3% of the streamflow decrease in JM from Period 1 (1965–1989) to Period 2 (1990–2003), which is similar to the results of previous studies in the study area (Zhao et al., 2009; Zheng et al., 2009). Furthermore, this study provides an explicit non-linear relationship between frozen ground degradation and streamflow changes in the SRYR (Fig. 6) and quantifies the streamflow response to frozen ground degradation (Table 5). The negative correlation between Q_{dev} and DDF_a supports the hypothesis that frozen ground degradation decreases streamflow in the TP (Cheng and Wu, 2007; Jin et al., 2009; Yang et al., 2010). As frozen ground degrades, the state point of (DDF_a, Q_{dev}) in Fig. 6 moves from the upper-right to the lower-left along the fitted curves. Frozen ground degradation decreases streamflow in the SRYR, but this decreasing effect gradually diminishes with the degradation stage. This deceleration was more obvious in the permafrost-dominated JM, and it initiated in 1995 when DDF_a dropped below 2100 °C-day. Since 1995, the air temperature has abruptly increased by 0.63 °C/10a. As stated in Duan et al. (2017b), the resulting increase in the active layer thickness and the thawing of permafrost might have contributed to the annual streamflow and caused the diminished decreasing effects of frozen ground degradation on the annual streamflow.

After quantifying the impacts of frozen ground degradation on the annual streamflow, the possible mechanisms of those impacts are discussed as follows. Since Q_{dev} reflects the deviation between the observed and Budyko-estimated annual streamflow (Q_{dev}=Q-Q_{Budyko}) caused by landscape factors including the frozen ground, it can be further decomposed into water storage changes (ΔS) and deviations between the actual and Budyko-estimated ET (ET_{dev} = $ET - ET_{Budyko}$) (Eq. (7), $Q_{dev} = -ET_{dev} - \Delta S$). The calculation of Q_{dev} does not rely on the values of actual ET, while the decomposition of Q_{dev} relies on the values of actual ET. Two different ET products, i.e., GLEAM and GBEHM, are adopted in this study, and they use different precipitation forcings; a comparison between those forcings can be found in Fig. S5. To investigate the different mechanisms between permafrost- and seasonally frozen ground-dominated regions, this section divides the entire SRYR into the permafrost dominated region upstream of Jimai station (JM, with 63.0% area underlain by permafrost) and seasonally frozen ground dominated region between Jimai and Tangnaihai station (JM-TNH, with only 17.3% area underlain by permafrost).

The decadal changes in Q_{dev} and its two components: ΔS and ET_{dev} during 1981–2010 in the SRYR are shown in Fig. 7. The decadal changes in DDF_a and the mean annual LAI are also shown in Fig. 7. The median values of Q_{dev} that represent the deviation between the observed and Budyko-estimated Q (Q_{dev} = $Q - Q_{Budyko}$) continued to decrease and became less than zero in the 2000s in both regions, indicating that landscape factors caused the stream-

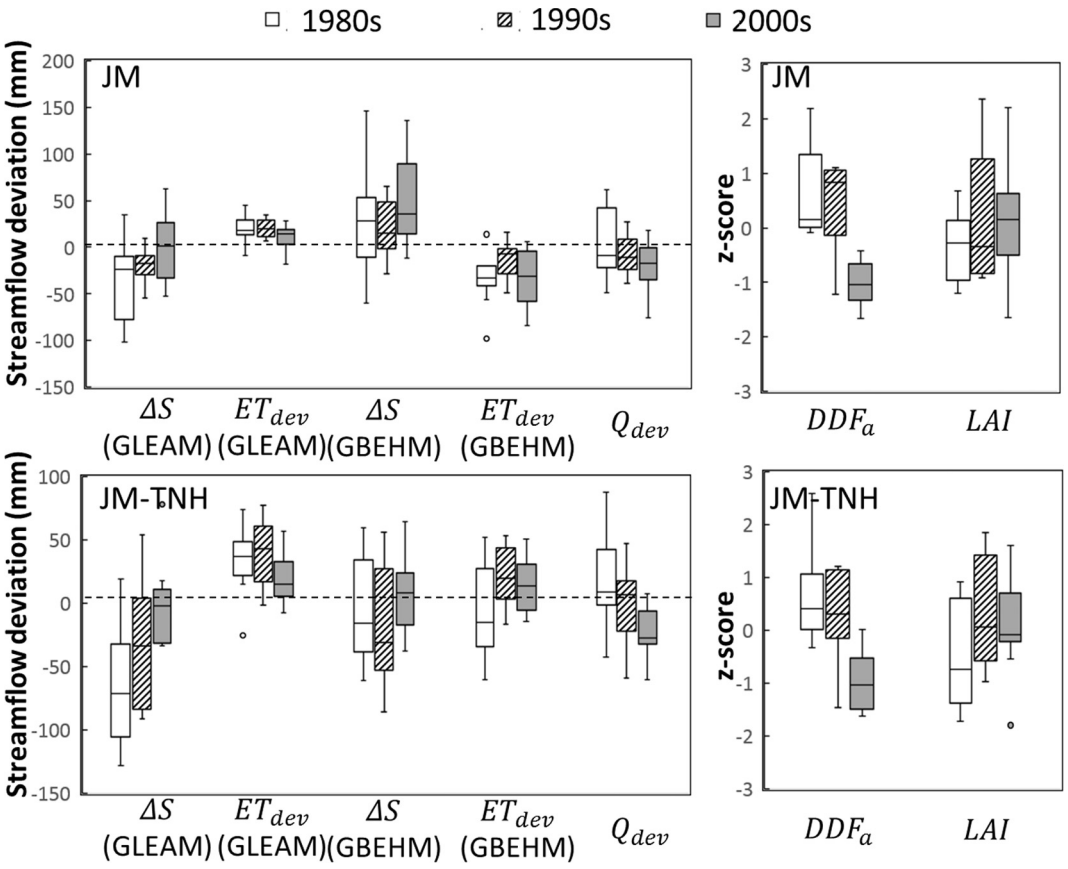

Fig. 7. Boxplots of ΔS and ET_{dev} derived from GLEAM and GBEHM, Q_{dev}, DDF_a and LAI in the 1980s, 1990s and 2000s in SRYR.

flow to become lower than the Budyko-based estimates during the 2000s. This phenomenon was caused by an increase in ΔS rather than an increase in ET_{dev}, which holds for both GLEAM and GBEHM, and it may have been related to the rapid decrease in DDF_a from the 1990s to the 2000s (Fig. 7).

An increase in ΔS within the SRYR subsequent to 2002 was also found using GRACE data, especially in those areas underlain by permafrost (Xu et al., 2013). These findings are consistent with the hypothesis that permafrost degradation decreases streamflow by enlarging the water storage capacity with an increasing active layer thickness (Niu et al., 2016) and that permafrost may even degrade into seasonally frozen ground and cause more water to percolate into deep aquifers, thereby increasing the groundwater storage (Qin et al., 2017). An increase in the active layer thickness and the thawing of permafrost might have contributed to the annual streamflow since the 2000s. However, the increase in ΔS exerted a greater impact on streamflow, which could have counteracted the increase in streamflow and caused the streamflow to decrease. These combined changes ultimately resulted in a diminished decreasing impact of frozen ground degradation on the annual streamflow, as is shown in Fig. 6.

6. Conclusions

In this study, long-term streamflow variations in the source region of the Yellow River (SRYR) were analyzed and attribution analysis within the Budyko framework was employed to quantify the streamflow response to the direct impact of climate change, the impact of frozen ground degradation, and land use change. According to the results, the following conclusions can be drawn.

1) The past 50 years can be divided into 3 sub-periods: Period 1 (P1, 1965–1989), Period 2 (P2, 1990–2003) and Period 3 (P3, 2004–2015). For the entire SRYR, the annual streamflow showed an insignificant decreasing trend (−6.51 mm/10a) during 1965–2015 in contrast to the insignificant increasing annual precipitation trend (+6.48 mm/10a) at the 0.05 significance level.
2) From P1 to P2, the direct impact of climate change can explain only 55.0% of the streamflow decrease for the entire SRYR. Frozen ground degradation can explain an additional 32.6% of the streamflow decrease in the SRYR during the same period. In the permafrost-dominated region upstream of the Jimai hydrological station, frozen ground degradation can explain 70.7% of the observed streamflow decrease.
3) From P2 to P3, the streamflow did not increase as much as the precipitation; this disparity could be attributable to the combined effects of an increasing potential evapotranspiration ($\Delta QE_0 = -5.1$ mm) and more importantly to frozen ground degradation ($\Delta Q_f = -13.1$ mm). The direct impact of climate change and the impact of frozen ground degradation can collectively explain 87.5% of the streamflow change from P2 to P3 for the entire SRYR.
4) Frozen ground degradation could reduce streamflow by increasing groundwater storage when the active layer thickness increases in a permafrost region.

The methods developed in this study can be used in other catchments as well to help develop a better understanding of the impacts of frozen ground degradation on water resources in the TP.

Acknowledgments

This research was supported by the National Natural Science Foundation of China (grant no. 41630856 and 91425303) and the National Program for Support of Top-Notch Young Professionals. The authors thank the three anonymous reviewers, the Editor and the Associate Editor for their constructive and detailed comments.

Appendix A. Supplementary data

Supplementary data associated with this article can be found, in the online version, at https://doi.org/10.1016/j.jhydrol.2018.01.050.

References

Arora, V.K., 2002. The use of the aridity index to assess climate change effect on annual runoff. J. Hydrol. 265 (1–4), 164–177. https://doi.org/10.1016/s0022-1694(02)00101-4.
Barnhart, T.B. et al., 2016. Snowmelt rate dictates streamflow. Geophys. Res. Lett. 43 (15), 8006–8016.
Beck, H.E. et al., 2017. MSWEP: 3-hourly 0.25 global gridded precipitation (1979–2015) by merging gauge, satellite, and reanalysis data. Hydrol. Earth Syst. Sci. 21 (1), 589.
Bense, V.F., Kooi, H., Ferguson, G., Read, T., 2012. Permafrost degradation as a control on hydrogeological regime shifts in a warming climate. J. Geophys. Res. Earth Surf. 117 (F3). https://doi.org/10.1029/2011jf002143.
Berghuijs, W.R., Woods, R.A., Hrachowitz, M., 2014. A precipitation shift from snow towards rain leads to a decrease in streamflow. Nat. Clim. Chang. 4 (7), 583–586. https://doi.org/10.1038/nclimate2246.
Budyko, M., 1974. Climate and Life (508pp). Academic Press, New York.
Cao, J., Qin, D., Kang, E., Li, Y., 2006. River discharge changes in the Qinghai-Tibet Plateau. Chin. Sci. Bull. 51 (5), 594–600.
Cheng, G.D., Wu, T.H., 2007. Responses of permafrost to climate change and their environmental significance, Qinghai-Tibet Plateau. J. Geophys. Res. Earth Surf. 112 (F2). https://doi.org/10.1029/2006jf000631.
Cuo, L. et al., 2015. Frozen soil degradation and its effects on surface hydrology in the northern Tibetan Plateau. J. Geophys. Res.-Atmos. 120 (16), 8276–8298. https://doi.org/10.1002/2015jd023193.
Donohue, R., Roderick, M., McVicar, T.R., 2010. Can dynamic vegetation information improve the accuracy of Budyko's hydrological model? J. Hydrol. 390 (1), 23–34.
Duan, L., Man, X., Kurylyk, B.L., Cai, T., 2017a. Increasing winter baseflow in response to permafrost thaw and precipitation regime shifts in northeastern China. Water 9 (1), 25.
Duan, L., Man, X., Kurylyk, B.L., Cai, T., Li, Q., 2017b. Distinguishing streamflow trends caused by changes in climate, forest cover, and permafrost in a large watershed in northeastern China. Hydrolog. Process. 31 (10), 1938–1951. https://doi.org/10.1002/hyp.11160.
Fang, Y.P., Qin, D.H., Ding, Y.J., 2011. Frozen soil change and adaptation of animal husbandry: a case of the source regions of Yangtze and Yellow Rivers. Environ. Sci. Policy 14 (5), 555–568. https://doi.org/10.1016/j.envsci.2011.03.012.
Frauenfeld, O.W., Zhang, T.J., McCreight, J.L., 2007. Northern hemisphere freezing/thawing index variations over the twentieth century. Int. J. Climatol. 27 (1), 47–63. https://doi.org/10.1002/joc.1372.
Fu, B., 1981. On the calculation of the evaporation from land surface. Sci. Atmos. Sin 5 (1), 23–31.
Gao, B., Qin, Y., Wang, Y., Yang, D., Zheng, Y., 2016. Modeling ecohydrological processes and spatial patterns in the upper heihe basin in China. Forests 7 (1), 10. https://doi.org/10.3390/f7010010.
Guo, D., Wang, H., 2013. Simulation of permafrost and seasonally frozen ground conditions on the Tibetan Plateau, 1981–2010. J. Geophys. Res.: Atmos. 118 (11), 5216–5230.
Hu, Y.R., Maskey, S., Uhlenbrook, S., Zhao, H.L., 2011. Streamflow trends and climate linkages in the source region of the Yellow River. China. Hydrol. Processes 25 (22), 3399–3411. https://doi.org/10.1002/hyp.8069.
Immerzeel, W.W., van Beek, L.P.H., Bierkens, M.F.P., 2010. Climate change will affect the Asian water towers. Science 328 (5984), 1382–1385. https://doi.org/10.1126/science.1183188.
Jarvis, A., Reuter, H.I., Nelson, A., Guevara, E., 2008. Hole-filled seamless SRTM data V4, International Centre for Tropical Agriculture (CIAT).
Jin, H.J. et al., 2009. Changes in frozen ground in the Source Area of the Yellow River on the Qinghai-Tibet Plateau, China, and their eco-environmental impacts. Environ. Res. Lett. 4 (4). https://doi.org/10.1088/1748-9326/4/4/045206.
Kang, S.C. et al., 2010. Review of climate and cryospheric change in the Tibetan Plateau. Environ. Res. Lett. 5 (1). https://doi.org/10.1088/1748-9326/5/1/015101.
Klene, A.E., Nelson, F.E., Shiklomanov, N.I., Hinkel, K.M., 2001. The n-factor in natural landscapes: variability of air and soil-surface temperatures, Kuparuk River basin, Alaska. USA. Arct. Antarct. Alp. Res. 33 (2), 140–148. https://doi.org/10.2307/1552214.
Landerer, F.W., Swenson, S.C., 2012. Accuracy of scaled GRACE terrestrial water storage estimates. Water Resour. Res. 48, 11. https://doi.org/10.1029/2011wr011453.
Li, J. et al., 2017. Grassland restoration reduces water yield in the headstream region of Yangtze River. Sci Rep 7, 9. https://doi.org/10.1038/s41598-017-02413-9.
Lyon, S.W., Destouni, G., 2010. Changes in catchment-scale recession flow properties in response to permafrost thawing in the Yukon River Basin. Int. J. Climatol. 30 (14), 2138–2145.
Meng, F., Su, F., Yang, D., Tong, K., Hao, Z., 2016. Impacts of recent climate change on the hydrology in the source region of the Yellow River basin. J. Hydrol.: Regional Stud. 6, 66–81.
Miralles, D.G. et al., 2014. El Niño–La Niña cycle and recent trends in continental evaporation. Nat. Clim. Chang. 4 (2), 122–126.
Ning, T., Li, Z., Liu, W., 2017. Vegetation dynamics and climate seasonality jointly control the interannual catchment water balance in the Loess Plateau under the Budyko framework. Hydrol. Earth Syst. Sci. 21 (3), 1515.
Niu, L. et al., 2016. Response of hydrological processes to permafrost degradation from 1980 to 2009 in the Upper Yellow River Basin. China. Hydrol. Res. 47 (5), 1014–1024. https://doi.org/10.2166/nh.2016.096.
Ol'Dekop, E., 1911. On evaporation from the surface of river basins. Trans. Meteorolog. Obs. 4, 200.
Peng, X. et al., 2017. Response of seasonal soil freeze depth to climate change across China. Cryosphere 11 (3), 1059.
Pike, J., 1964. The estimation of annual run-off from meteorological data in a tropical climate. J. Hydrol. 2 (2), 116–123.
Potter, N.J., Zhang, L., 2009. Interannual variability of catchment water balance in Australia. J. Hydrol. 369 (1), 120–129.
Qin, Y. et al., 2016. Long-term change in the depth of seasonally frozen ground and its ecohydrological impacts in the Qilian Mountains, northeastern Tibetan Plateau. J. Hydrol. 542, 204–221.
Qin, Y. et al., 2017. Impacts of climate warming on the frozen ground and eco-hydrology in the Yellow River source region. China. Sci. Tot. Environ. 605–606, 830–841. https://doi.org/10.1016/j.scitotenv.2017.06.188.
Qiu, J., 2008. China: the third pole. Nature 454 (7203), 393–396.
Qiu, J., 2012. Thawing permafrost reduces river runoff. Nature.
Ran, Y.H. et al., 2012. Distribution of permafrost in china: an overview of existing permafrost maps. Permafr. Periglac. Proc. 23 (4), 322–333. https://doi.org/10.1002/ppp.1756.
Sato, Y. et al., 2008. Analysis of long-term water balance in the source area of the Yellow River basin. Hydrol. Processes 22 (11), 1618–1629. https://doi.org/10.1002/hyp.6730.
Schreiber, P., 1904. Über die Beziehungen zwischen dem Niederschlag und der Wasserführung der Flüsse in Mitteleuropa. Z. Meteorol 21 (10), 441–452.
Shen, Y., Xiong, A., 2016. Validation and comparison of a new gauge-based precipitation analysis over mainland China. Int. J. Climatol. 36 (1), 252–265. https://doi.org/10.1002/joc.4341.
Shuttleworth, W., 1993. Evaporation. Handbook of Hydrology. McGraw-Hill.
Walvoord, M.A., Kurylyk, B.L., 2016. Hydrologic impacts of thawing permafrost-A review. Vadose Zone J. 15 (6), 20. https://doi.org/10.2136/vzj2016.01.0010.
Wang, D., Hejazi, M., 2011. Quantifying the relative contribution of the climate and direct human impacts on mean annual streamflow in the contiguous United States. Water Resour. Res. 47. https://doi.org/10.1029/2010wr010283.
Wang, Q.F., Zhang, T.J., Peng, X.Q., Cao, B., Wu, Q.B., 2015. Changes of soil thermal regimes in the Heihe River Basin over Western China. Arct. Antarct. Alp. Res. 47 (2), 231–241. https://doi.org/10.1657/aaar00c-14-012.
Wang, X., Chen, R., Yang, Y., 2017. Effects of Permafrost degradation on the hydrological regime in the source regions of the Yangtze and Yellow Rivers. China. Water 9 (11), 897.
Wu, Q.B., Hou, Y.D., Yun, H.B., Liu, Y.Z., 2015. Changes in active-layer thickness and near-surface permafrost between 2002 and 2012 in alpine ecosystems, Qinghai-Xizang (Tibet) Plateau. China. Global Planet. Change 124, 149–155. https://doi.org/10.1016/j.gloplacha.2014.09.002.
Xu, H., Wang, X.-P., Zhang, X.-X., 2016. Alpine grasslands response to climatic factors and anthropogenic activities on the Tibetan Plateau from 2000 to 2012. Ecological Engineering 92, 251–259.
Xu, M., Ye, B., Zhao, Q., Zhang, S., Wang, J., 2013. Estimation of water balance in the source region of the Yellow River based on GRACE satellite data. J. Arid Land 5 (3), 384–395. https://doi.org/10.1007/s40333-013-0169-8.
Xu, X., Yang, D., Yang, H., Lei, H., 2014. Attribution analysis based on the Budyko hypothesis for detecting the dominant cause of runoff decline in Haihe basin. J. Hydrol. 510, 530–540. https://doi.org/10.1016/j.jhydrol.2013.12.052.
Yang, D. et al., 2004. Analysis of water resources variability in the Yellow River of China during the last half century using historical data. Water Resour. Res. 40 (6). https://doi.org/10.1029/2003wr002763.
Yang, D.W. et al., 2007. Analyzing spatial and temporal variability of annual water-energy balance in nonhumid regions of China using the Budyko hypothesis. Water Resour. Res. 43 (4), 12. https://doi.org/10.1029/2006wr005224.
Yang, H., Qi, J., Xu, X., Yang, D., Lv, H., 2014. The regional variation in climate elasticity and climate contribution to runoff across China. J. Hydrol. 517, 607–616.
Yang, H., Yang, D., 2011. Derivation of climate elasticity of runoff to assess the effects of climate change on annual runoff. Water Resour. Res. 47 (7).
Yang, H., Yang, D., Lei, Z., Sun, F., 2008. New analytical derivation of the mean annual water-energy balance equation. Water Resour. Res. 44 (3). https://doi.org/10.1029/2007wr006135.

Yang, K. et al., 2011. Response of hydrological cycle to recent climate changes in the Tibetan Plateau. Clim. Change 109 (3–4), 517–534. https://doi.org/10.1007/s10584-011-0099-4.

Yang, M.X., Nelson, F.E., Shiklomanov, N.I., Guo, D.L., Wan, G.N., 2010. Permafrost degradation and its environmental effects on the Tibetan Plateau: a review of recent research. Earth-Sci. Rev. 103 (1–2), 31–44. https://doi.org/10.1016/j.earscirev.2010.07.002.

Yang, Y., Donohue, R.J., McVicar, T.R., Roderick, M.L., Beck, H.E., 2016. Long-term CO2 fertilization increases vegetation productivity and has little effect on hydrological partitioning in tropical rainforests. J. Geophys. Res.: Biogeosci. 121 (8), 2125–2140.

Yi, S., Wang, X., Qin, Y., Xiang, B., Ding, Y., 2014. Responses of alpine grassland on Qinghai-Tibetan plateau to climate warming and permafrost degradation: a modeling perspective. Environ. Res. Lett. 9 (7). https://doi.org/10.1088/1748-9326/9/7/074014.

Yin, Y.Y., Liu, H., Yi, X.S., Liu, W.D., 2015. Spatiotemporal Variation and Abrupt Change Analysis of Temperature from 1960 to 2012 in the Huang-Huai-Hai Plain, China. Adv. Meteorol. 11. https://doi.org/10.1155/2015/643493.

Yuan, F.F. et al., 2015. Hydro climatic trend and periodicity for the source region of the Yellow River. J. Hydrol. Eng. 20 (10). https://doi.org/10.1061/(asce)he.1943-5584.0001182.

Zhang, D., Cong, Z., Ni, G., Yang, D., Hu, S., 2015. Effects of snow ratio on annual runoff within the Budyko framework. Hydrol. Earth Syst. Sci. 19 (4), 1977–1992. https://doi.org/10.5194/hess-19-1977-2015.

Zhang, L., Dawes, W., Walker, G., 2001. Response of mean annual evapotranspiration to vegetation changes at catchment scale. Water Resour. Res. 37 (3), 701–708.

Zhang, S.L., Yang, H.B., Yang, D.W., Jayawardena, A.W., 2016a. Quantifying the effect of vegetation change on the regional water balance within the Budyko framework. Geophys. Res. Lett. 43 (3), 1140–1148. https://doi.org/10.1002/2015gl066952.

Zhang, W.J., Yi, Y.H., Song, K.C., Kimball, J.S., Lu, Q.F., 2016b. Hydrological response of alpine wetlands to climate warming in the Eastern Tibetan Plateau. Remote Sens.-Basel 8 (4). https://doi.org/10.3390/rs8040336.

Zhang, X.S., Srinivasan, R., Debele, B., Hao, F.H., 2008. Runoff simulation of the headwaters of the Yellow River using the SWAT model with three snowmelt algorithms. J. Am. Water Resour. Assoc. 44 (1), 48–61. https://doi.org/10.1111/j.1752-1688.2007.00137.x.

Zhang, Y. et al., 2016c. Multi-decadal trends in global terrestrial evapotranspiration and its components. Sci. Rep. 6 (6).

Zhao, F.F., Xu, Z.X., Zhang, L., Zuo, D.P., 2009. Streamflow response to climate variability and human activities in the upper catchment of the Yellow River Basin. Sci. China Ser. E-Technol. Sci. 52 (11), 3249–3256. https://doi.org/10.1007/s11431-009-0354-3.

Zheng, H.X., Zhang, L., Liu, C.M., Shao, Q.X., Fukushima, Y., 2007. Changes in stream flow regime in headwater catchments of the Yellow River basin since the 1950s. Hydrol. Processes 21 (7), 886–893. https://doi.org/10.1002/hyp.6280.

Zheng, H.X. et al., 2009. Responses of streamflow to climate and land surface change in the headwaters of the Yellow River Basin. Water Resour. Res. 45, 9. https://doi.org/10.1029/2007wr006665.

Zhou, G. et al., 2015a. Global pattern for the effect of climate and land cover on water yield. Nat. Commun. 6.

Zhou, S., Yu, B., Huang, Y., Wang, G., 201b. The complementary relationship and generation of the Budyko functions. Geophys. Res. Lett. 42 (6), 1781–1790. https://doi.org/10.1002/2015gl063511.

Zhu, Z. et al., 2013. Global Data Sets of Vegetation Leaf Area Index (LAI)3g and Fraction of Photosynthetically Active Radiation (FPAR)3g Derived from Global Inventory Modeling and Mapping Studies (GIMMS) Normalized Difference Vegetation Index (NDVI3g) for the Period 1981 to 2011. Remote Sensing 5 (2), 927. https://doi.org/10.3390/rs5020927.